Front. Optoelectron. 2012, 5(1): 41–50
DOI 10.1007/s12200-012-0200-2

REVIEW ARTICLE

Ge-on-Si for Si-based integrated materials and photonic devices

Weixuan HU, Buwen CHENG (✉), Chunlai XUE, Shaojian SU, Haiyun XUE, Yuhua ZUO, Qiming WANG

State Key Laboratory on Integrated Optoelectronics, Institute of Semiconductors, Chinese Academy of Sciences, Beijing 100083, China

© Higher Education Press and Springer-Verlag Berlin Heidelberg 2012

Abstract This paper reviews the recent progress in photonic devices application of Ge-on-Si. Ge-on-Si materials and optical devices are suitable candidates for Si-based optoelectronic integration because of the mature epitaxial technique and the compatibility with Si complementary metal-oxide-semiconductor (CMOS) technology. Recently, the realities of electric-pump Ge light emitting diode (LED) and optical-pump pulse Ge laser, Ge quantum well modulator based on quantum Stark confined effect, waveguide Ge modulator based on Franz-Keldysh (FK) effect, and high performance near-infrared Ge detector, rendered the Si-based optoelectronic integration using Ge photonic devices. Ge-on-Si material is also an important platform to grow other materials on it for Si-based optoelectronic integration. InGaAs and GeSn have been grown on the Ge-on-Si. InGaAs LED and GeSn photodetector have been successfully fabricated as well.

Keywords optoelectronic integration, Ge, photonic device

1 Introduction

Si is a kind of dominated semiconductor material for electronic industry. It is an inexpensive, well understood material, with a naturally high quality adhering oxide SiO_2, stable chemical and electrical properties. In 1970, high speed, long distance data transmission with low loss and low dispersion became achieved using fiber as medium. Since then, photonic devices monolithic integrated on Si have attracted remarkable interest because of the transparency in optical communication wavelengths of Si and its compatibility with Si complementary metal-oxide-semiconductor (CMOS) technique. Si-based optoelectronic integrated circuit (OEIC) covers the devices in the following fields: (1) The propagation of light. Si provides strong optical confinement for optical communication wavelengths when incorporated into waveguide structures, such as silicon-on-insulator (SOI). Thus, the Si waveguides, couplers, wavelength division multiplexers, etc., have successfully been fabricated. (2) The generation of light. It's difficult since Si is an indirect bandgap semiconductor which leads to poor light-emitting. Although Intel Corporation and University of California at Santa Barbara demonstrated an InP-based laser bonding on Si [1], the incompatibility of III-V technique with Si industry makes the hybrid InP laser difficulty in commercial application. Groups at University of California, Los Angeles (UCLA) and Inter Corporation developed Si Raman laser [2,3], which is fully compatible with Si electronic circuits and offers tenability by design. However, the device needs optical pumping. Till now, electric pump Si-based high-efficiency light source operating at room temperature is still the main challenge in Si photonics. (3) The photodetector. The Si detector shows high performance at wavelengths shorter than 1 μm, thus the optical communication wavelengths are not covered by the device. (4) The light modulation. For Si, the Pockels effect does not exist, besides Kerr effect and Franz-Keldysh (FK) effect are extremely low [4]. Recent years, lots of work have been done using the carrier plasma dispersion effect with Mach-Zehnder interferometer (MZI) or microring structures. The MZI modulator has a disadvantage of large device size. The microring resonator modulator suffers from high temperature sensitivity. In order to realize optoelectronic integration on Si, many efforts have been made to combine other materials with good optical characteristics on Si substrate.

Ge has many advantageous properties comparing with Si. Ge has higher bulk mobility for both electrons and holes: The electron mobility is $3900\,cm^2 \cdot V^{-1} \cdot s^{-1}$ for Ge and $1417\,cm^2 \cdot V^{-1} \cdot s^{-1}$ for Si, while the hole mobility is $1900\,cm^2 \cdot V^{-1} \cdot s^{-1}$ for Ge and $471\,cm^2 \cdot V^{-1} \cdot s^{-1}$ for Si. What's more, the direct bandgap of Ge (E_Γ = 0.8 eV) is exactly corresponding to optical communication wave-

Received September 30, 2011; accepted November 15, 2011

E-mail: cbw@semi.ac.cn

length 1550 nm. Although Ge is also a direct bandgap material, the direct bandgap E_{Γ} is only 140 meV larger than the indirect bandgap at L valley (E_L = 0.66 eV). The light emitting property of Ge can be improved by tensile straining and n-type doping to increase the electron occupation probability at Γ valley. So, integrating Ge with Si to fabricate Ge photonic devices on Si substrate is a promising route for Si optoelectronic integration.

Despite the large lattice mismatch between Ge and Si, high quality Ge films have been grown on Si using the two-step strategy [5], in which the Ge buffer layer grown at low temperature relaxes most of the strain induced by the 4.2% lattice mismatch. Using the Ge-on-Si material, several high performance Ge photonic devices have been fabricated on Si substrate.

This paper reviews the recent progress of Ge photonic devices on Si for Si-based OEIC, such as the Ge photodetector, electric pump Ge light emitting diode (LED), the optical pump Ge laser, the Ge quantum well modulator based on the quantum confined Stark effect (QCSE) and the Ge modulator based on FK effect. Epitaxy of InGaAs and $Ge_{1-x}Sn_x$ alloy on the Ge-on-Si, which respectively enable the mature III-V technology and novel infrared detector on Si, are also introduced.

2 Ge-on-Si LED and laser

In 2007, Liu et al. theoretically demonstrated that, with proper band structure engineering using in-plain tensile stress and n-type doping, Ge can be used for efficient light emission and optical gain can be achieved near 1550 nm (corresponding to its direct bandgap E_{Γ} = 0.8 eV) [6]. Since then, lots of theoretical and experimental works have focused on this field. According to the deformation potential theory, Ge behaves more like the direct bandgap material under biaxial tensile strain [7]. The direct bandgap and indirect bandgap of Ge both shrink under biaxial tensile strain, but the former has larger shrinking rate than the latter. That is, for Ge: $dE_{\Gamma}/d\ln\Omega = -9.48$ eV, $dE_L/d\ln\Omega = -2.78$ eV. Here, $\ln\Omega = \Delta\Omega/\Omega$ is the volume change under biaxial strain. Calculations indicated that Ge will transform to be direct bandgap semiconductor under biaxial tensile strain larger than 2%. Cheng et al. observed the enhancement of direct bandgap photoluminescence induced by tensile strain [8]. The strain was induced by mechanical method. Under 0.37% in-plane tensile strain, the integrated intensity ratio between the direct and indirect bandgap photoluminescence can be enhanced by 1.8 times.

The purpose of the band engineering via n-type doping is to increase the Fermi level up to the bottom of the Γ valley of the conduction band. In this case, the energy states of the L valley, which is below the bottom of Γ valley, are already filled by electrons. As a result, higher direct bandgap radiative recombination rate is expected, and a much lower injected carrier density is needed to achieve the population inversion. The enhancement of direct bandgap photoluminescence induced by the indirect valley state filling effect was observed by Sun et al. [9].

Based on the theories mentioned above, several groups have fabricated Ge LEDs operating at room temperature [10,11]. The direct bandgap electroluminescence (EL) from Ge/Si heterojunction LED at room temperature was observed in the reports. Figure 1 shows the EL spectra of our Ge-on-Si LED. The electric-pumped light emission near 1565 nm was observed in a Ge/Si p-i-n device under forward bias range from 1.1 to 2.5 V. The injection current density of the device was 800 A/cm^2 under 1.1 V forward bias. The electric-pumped emission spectra were broad with a full width at half maximum (FWHM) of 90 meV. The emission mechanism was confirmed to be the radiative recombination from the Γ valley to the top of the valence band. Cheng et al. [12] demonstrated and discussed the thermal enhancement effect of EL spectra, and indicated the potential capability of the Ge laser to operate at room temperature.

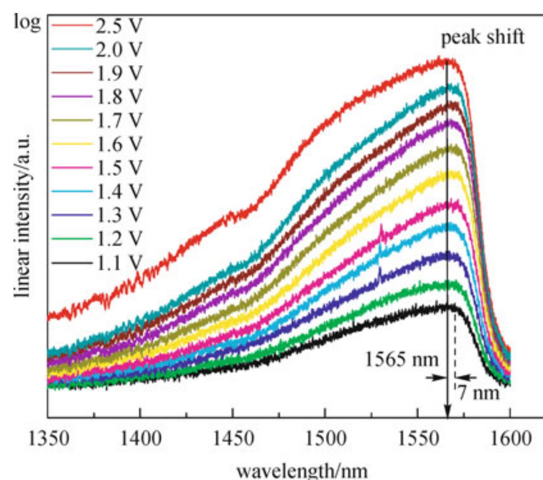

Fig. 1 EL spectra of the device. The bias was ranging from 1.1 to 2.5 V. The peak shift curve is also shown in the figure

In 2010, the first optical pumped Ge-on-Si laser operating at room-temperature was reported [13]. The device was fabricated by selectively growing 1.6 μm ×0.5 μm Ge waveguides on Si. The Ge layer was 0.24% biaxial tensile strain induced by the difference between the thermal expansion coefficient of Ge and Si. The Ge film was n-type phosphorous doped at a level of 1×10^{19} cm^{-3}, which allowed an enhancement of light emission from direct gap of 0.76 eV. The optically pumping source is a 1064 nm Q-switched laser of 1.5 ns pulse duration, with a mirror-polished and 4.8 mm long Fabry-Perot cavity. The peak pump power density absorbed by Ge film was estimated to be 300 kW/cm^2. A broad photoluminescence peak at 1600 nm was observed under pumping at 1.5 μJ per pulse, with emission peaks emerging at 1599, 1606 and 1612 nm.

3 Ge optical modulator on Si

Generally speaking, there are two kinds of Ge modulators: Ge-on-Si or Ge-on-SOI (Si on insulator) electro-absorption (EA) modulators based on FK effect, and on QCSE. Both of them are based on the change of the absorption coefficient under an external electric field.

The first waveguide-integrated GeSi EA modulator based on FK effect was fabricated by Liu et al. in 2008 [14]. In order to adjust the working wavelength into the C-band region (1528–1560 nm), they substitute $Ge_{0.925}Si_{0.075}$ for pure Ge in the device fabrication. The result indicated that the absorption coefficient changes abruptly within a large wavelength range. The GeSi EA modulator is 50 μm long, 600 nm wide and 400 nm high, correspondingly having an active area as small as 30 μm^2. Because of the small active area, the capacitance of the device is as low as 11 fF, thus leading to a low RC delaying factor. As a result, the bandwidth is theoretically higher than 50 GHz. In 2010, Feng et al. demonstrated a 30 GHz Ge EA modulator based on FK effect without scarifying other performances [15]. The device needs only 3 V reverse bias to achieve extinction ratio higher than 7dB in the wavelengths ranging from 1510 to 1552 nm. The energy consumption per bit is estimated to be only 50 fJ, which is much lower than that of their counterparts based on plasma dispersion effect.

Our group also has studied FK effect of a normal-incidence Ge-on-Si diode. The modulator has 800 nm active thickness, and has an incident surface of a circle with 25 μm radius. The absorption coefficients of Ge under different electric field are shown in Fig. 2, which enables the light modulation within 1620–1640 nm.

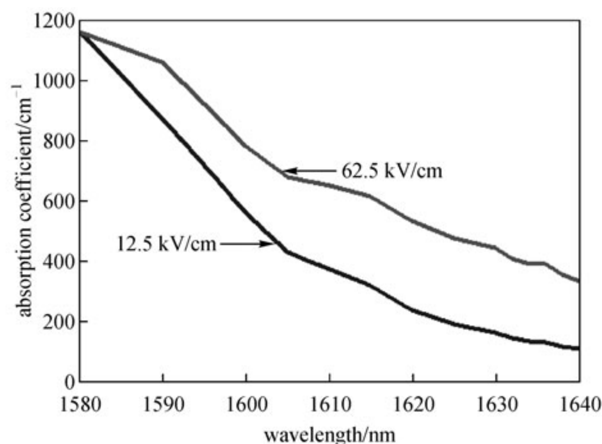

Fig. 2 Ge absorption coefficient spectra under external electric field of 12.5 and 62.5 kV/cm

QCSE is the special case of FK effect in multiple quantum wells (MQWs). The modulator based on QCSE also brings the merits of small device area, low power consumption and large bandwidth. In 2005, the QCSE of Ge/GeSi quantum wells was first reported by Kuo and Zhao et al. [16,17]. The results attracted considerable interest in the Ge quantum well modulators based on QCSE around the world. Recently, our group also observed the QCSE of Ge quantum well modulator. The active region of the modulator consisted of 10 pairs of Ge/ $Si_{0.15}Ge_{0.85}$ quantum wells. The Ge and $Si_{0.15}Ge_{0.85}$ layers were 18 and 27 nm thick, respectively. Figure 3 shows the photocurrent measurement results. The photocurrent spectrum is measured under different reverse voltages at room temperature. The random polarized light, tuned by a laser with the wavelength ranging from 1450 to 1550 nm, is incident normally to the surface of the modulator. The QCSE can be obviously seen from the photocurrent spectrum measurements. In Fig. 3(a), the absorption peak increases as the reverse bias raising from 0 to 1.5 V, implying that the intrinsic region is not fully depleted. Therefore, the photo-generated carriers can not be fully collected if the bias is below 1.5 V [18]. On the contrary in Fig. 3(b), the peak of the photocurrent decreased when the reverse bias increases from 1.5 to 3.0 V. In this case, the photocurrent reduction results from the decreased overlap between the electron and hole wave functions at reverse bias.

In 2010, Rong et al. demonstrated the Ge quantum well modulator with small-signal optical modulation speed up to 13 GHz [19]. The reason of the high modulation speed is the unique Ge energy structure and material properties. The strong quantum confinement occurs in the direct bandgap and carriers will fast lie in the lower indirect bandgap, without conventional thermal emission out of the quantum well which is the case for III-V materials.

4 High performance Ge-on-Si photodetector

Several groups have fabricated Ge photodetectors on Si with normal-incidence or waveguide structure. The normal-incidence Ge/Si photodetectors are mainly applied to free-space detection and fiber-optic coupling. On the other hand, the Ge waveguide photodetector plays an important role in Si-based optoelectronic integration and on-chip optical interconnection. The waveguide photodetector overcomes the trade-off between quantum efficiency and bandwidth, because the absorption length is decoupled from the carried collection path. So the waveguide Ge detector could have high responsivity and high speed simultaneously. Table 1 lists some typical reports of normal-incidence Ge/Si photodetectors. It can be found that the Ge PD with a bandwidth as high as 43 GHz was realized. But one must make a trade-off between responsivity and the speed. Figure 4 shows the cross-section structure of a normal-incidence Ge/Si (SOI) photodetector fabricated by our group [20]. For a 30 μm-diameter detector in our work, the optical responsivity at −1 V bias was 0.65 A/W at 1.31 μm and 0.31 A/W at

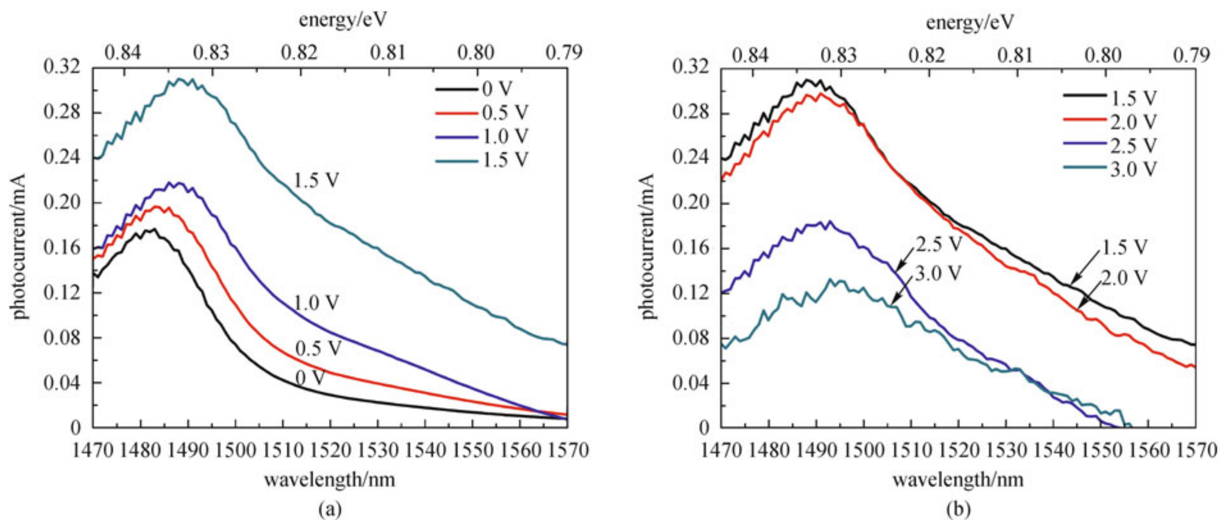

Fig. 3 Photocurrent spectrum of Ge quantum well modulator (with 10 pairs of 10 nm Ge wells and 18 nm $Si_{0.15}Ge_{0.85}$ barriers) with reverse bias from (a) 0 to 1.5 V and (b) 1.5 to 3.0 V

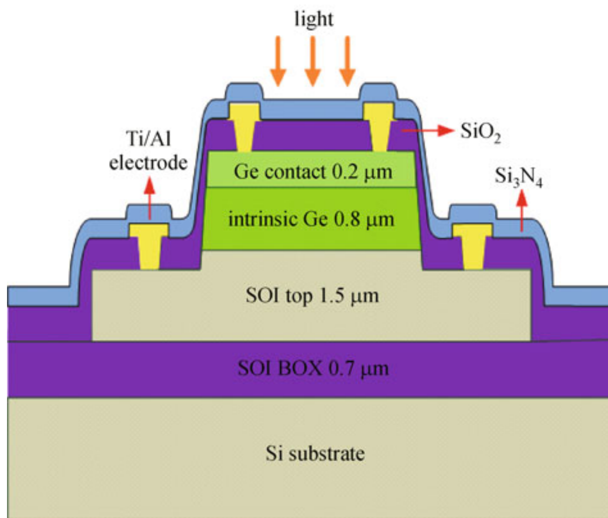

Fig. 4 Schematic cross-section view of double mesa structure of Ge p-i-n photodetector

1.55 μm. The dark current density of the device was 14.8 mA/cm^2 at –1V bias. The 3 dB bandwidth was 11.34 GHz at –1V bias and 12.60 GHz at –3 V bias.

Table 2 lists some recent typical reports of the waveguide Ge/Si photodetectors. The light from the waveguide can be coupled to the Ge active layer with a butt-couple or evanescent-couple configuration. For the evanescent-couple strategy, the waveguide can be on the top or bottom of the Ge detector. Intel Corporation fabricated a bottom p-i-n coupled waveguide Ge detector on Si in 2007 [27]. The Ge waveguide detector with a width of 7.4 μm and a length of 50 μm demonstrated an optical bandwidth of 31.3 GHz at –2 V for 1550 nm. At bias of –2 V, the responsivity was 0.89 A/W at 1550 nm and the dark current was 169 nA. The results indicated the device is a good candidate for high data rate applications including 40 Gb/s operation. In 2009, Feng et al. demonstrated the butt-coupled Ge waveguide detector on SOI [28]. The device used a top Si layer of SOI as waveguide, and the selectively-grown Ge layer as absorption region with area of 0.8 μm × 10 μm. The detector has a responsivity of 1.1 A/W and 3 dB bandwidth (3 dB BW) of 32 GHz at 1.55 μm.

The Ge/Si avalanche photodetectors (APDs) with separate absorption-charge-multiplication (SACM) structure combine the high optical absorption of Ge at optical-communication wavelengths with the excellent carrier multiplication of Si. In the Ge/Si SACM APDs, light is absorbed in an intrinsic-Ge (i-Ge) film and electrons are multiplied in a Si film. Due to the high responsivity and low noise, the devices are promising in the application of bio-photonics, optical communication, and quantum information science. Moreover, the Ge/Si APDs have advantages over their III-V counterparts in integration with Si. Intel corporation, University of California Santa Barbara and University of Virginia reported the Ge/Si APDs with 340 GHz gain-bandwidth product at 1300 nm in 2009 [31]. The sensitivity of the device was –28 dBm at 10 Gbs^{-1} at 1300 nm. For a 30 μm-diameter APD, the punch through voltage was about –22 V with a responsivity of 5.88 A/W at 1310 nm, and the breakdown voltage was about –25 V (defined at a dark current of 100 μA). The primary responsivity used to obtain gain was 0.55 A/W measured from p-i-i-n devices fabricated on the same wafer.

Our group demonstrated the Ge/Si SACM APDs in 2009 [32]. The cross-section structure of the device is shown in

Table 1 Performance comparison for different normal-incidence Ge photodetector designs

active Ge thickness/μm	R at 1550 nm/(A·W^{-1})	J_{dark}/(mA·cm^{-2})	3 dB BW	year
3.8	0.75	15 (−1V)	~2.5 GHz	2002 [21]
2.35	0.52	11 (−1V)		2005 [22]
1.3	0.2	~200 (−1V)	10 Gbit/s	2006 [23]
0.3	0.04	100 (−1V)	~43 GHz	2007 [24]
0.6	0.1	8.65 (−1V)	–	2009 [25]
0.6	0.24	3.98 (−1V)	6.28 GHz	2009 [26]
0.8	0.31	14.8(−1V)	12.6GHz	2010 [20]

Table 2 Performance comparison for different waveguide Ge photodetector designs

device structure	R at 1.55 μm/(A·W^{-1})	I_{dark}/μA	3 dB BW	year
butt, MSM	1±0.2	130	25 at −6V	2007 [29]
top, PIN	0.87	0.9	7.2	2007 [30]
bottom, PIN	0.89	0.17 at −2V	31.3 at −2V	2007 [27]
butt, PIN	1.1	1.3	32	2009 [28]

Fig. 5. For a 30 μm-diameter APD, the punch through voltage was about −29 V and the breakdown voltage was about −39.5 V (defined at a dark current of 100 μA). The photocurrents of a typical 30 μm-diameter device were measured at different optical power as shown in Fig. 6. The optical power was changed by optical attenuator from −10 to −35 dBm. Even when the optical power is as low as −35 dBm, the device still had good photocurrent performance. The device has a responsivity of 4.4 A/W at 1310 nm when biased at 90% breakdown voltage. The measured multiplication gain as a function of bias at 1310 nm was exhibited in Fig. 7, with the primary responsivity of 0.5 A/W. The APD exhibited a gain of 8.8 at 1310 nm when biased at 90% breakdown voltage.

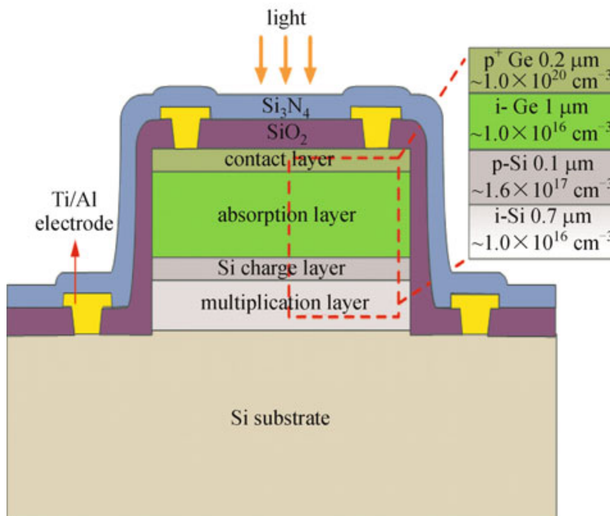

Fig. 5 Schematic cross-section view of Ge/Si SACM APD

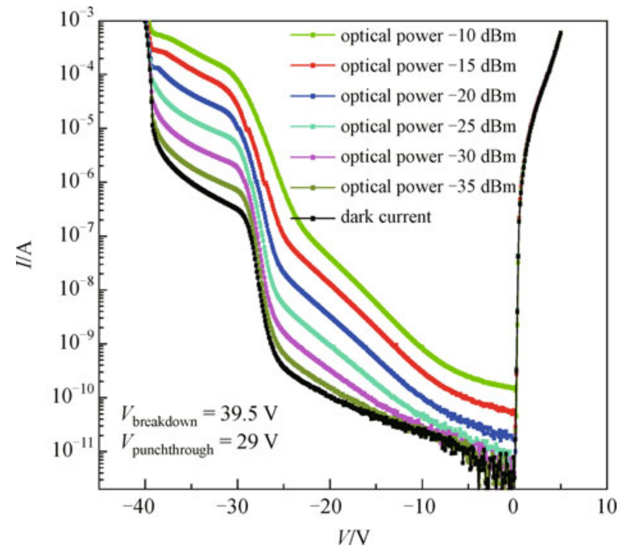

Fig. 6 *I-V* characteristics at darkness and with illumination by 1310 nm light of 30 μm-diameter detector for different illuminate optical power

5 Epitaxy of III-V materials on Ge/Si and InGaAs LED on Si

Epitaxy of GaAs on Si enables the III-V devices integrated on Si substrate of commercial wafer-scale. However, there are four main challenges in the growth of GaAs on Si [33]: (1) lattice mismatch between GaAs and Si; (2) formation of anti-phase boundary (APB) on GaAs side of the interface; (3) lack of electrical neutrality at the interface; (4) cross-doping between GaAs and Si. Epitaxy of GaAs on offcut Si substrate using Ge as buffer layer avoids the GaAs/Si lattice mismatch and the formation of APBs at the same

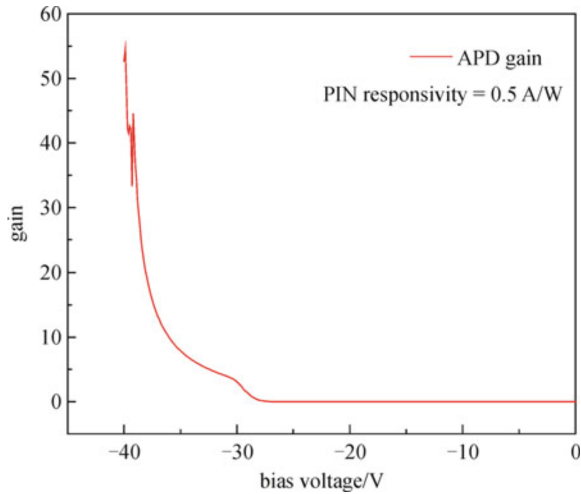

Fig. 7 Measured multiplication gain as a function of bias at a wavelength of 1310 nm. The primary photoresponsivity used to obtain gain is 0.50 A/W measured from Ge p-i-n devices fabricated with the same Ge thickness

time. This technique is important in the field of III-V laser integrated on Si and GaAs/Ge/Si multijunction solar cells.

The study of Beeler et al. in 2010 compared the growth of GaAs on bulk Ge and on virtual Ge/Si(100) substrates for photovoltaic applications [34]. The Ge layers were grown using the gas source of the combination of $CH_2(GeH_3)_2$ additives with large amounts of Ge_2H_6. GaAs films were grown, respectively, via Ge layers on 5° offcut Si(100) substrate and on 5° offcut Ge(100) wafer. High quality GaAs films with smooth surface and extremely low threading dislocation were obtained in both cases. However, the GaAs on Ge wafer showed the better performances comparing with the GaAs layer on Ge/Si(100) under the same conditions.

Recently, our group has investigated the growth of $In_{0.01}Ga_{0.99}As$ on 6° offcut Si(100) substrate using Ge as buffer layers. The Ge layers were grown by ultrahigh vacuum chemical vapor deposition using a “low/high temperature” strategy, while the $In_{0.01}Ga_{0.99}As$ layers were grown by metal-organic chemical vapor deposition. The

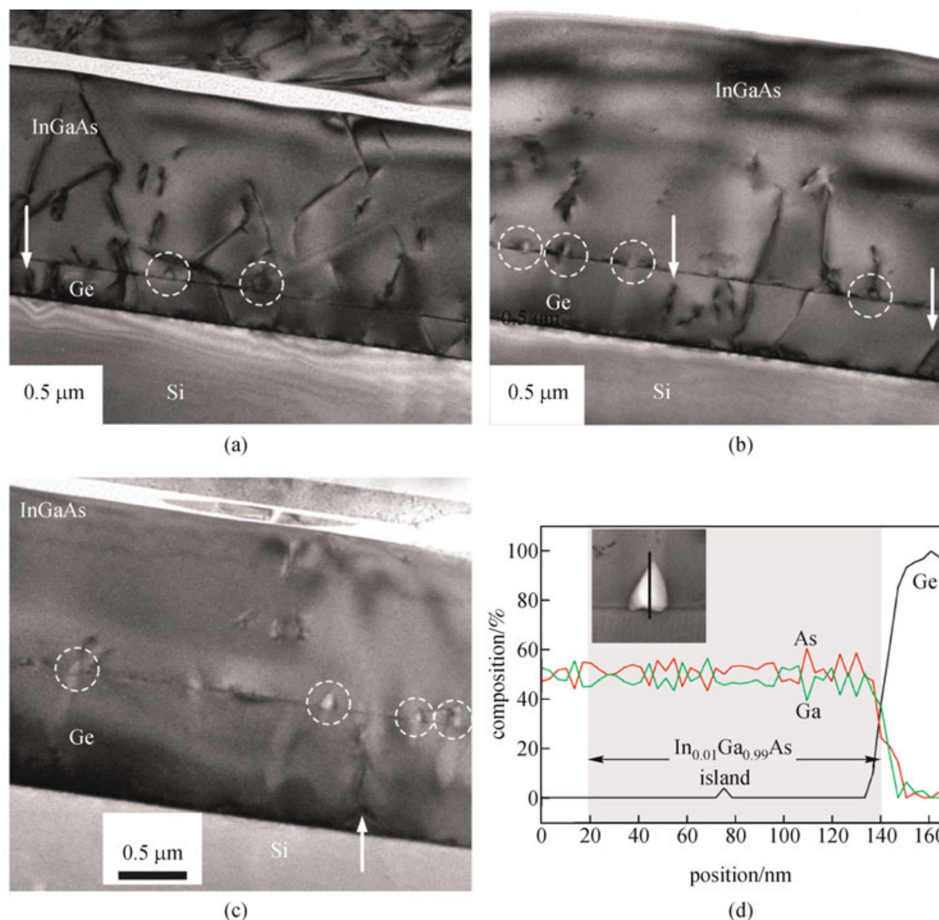

Fig. 8 Cross section TEM images of $In_{0.01}Ga_{0.99}As$ on (a) 300nm, (b) 550 nm and (c) 1020 nm Ge/offcut Si(001) virtual substrate. The GaAs islands on $In_{0.01}Ga_{0.99}As$/Ge interface are indicated by dash circles. The solid arrows show the TD reduction in Ge/offcut Si. In inset (d), the EDS along the black line through a GaAs island is shown

$In_{0.01}Ga_{0.99}As$ layer was free of APB, the R_{rms} (root mean square roughness) was about 4 nm, and the threading dislocation density was about 10^5 cm^{-2}. The transmission electron microscope (TEM) images of three $In_{0.01}Ga_{0.99}As$/Ge/Si samples are shown in Fig. 8, the thickness of the Ge buffer layer is (a) 300 nm, (b) 550 nm and (c) 1020 nm, respectively.

We have successfully fabricated $In_{0.01}Ga_{0.99}As$ LEDs on offcut Si substrate. The schematic cross-section view of the LED is shown in Fig. 9. The top 0.4 μm $In_{0.01}Ga_{0.99}As$ layer was 10^{19} cm^{-3} p^+-type doping, and the bottom 1.1 μm $In_{0.01}Ga_{0.99}As$ layer was 5×10^{18} cm^{-3} n^--type doping. The EL spectrum at room temperature of the $In_{0.01}Ga_{0.99}As$/Ge/Si LED with mesa diameter of 200 μm is shown in Fig. 10. The injection current was kept constant in the level of 50 mA. Because of the power consumption during the measurement, the peak of the EL spectra was red shifted to about 900 nm. The results indicated the high performance III-V device on Si with the aid of high quality Ge layer.

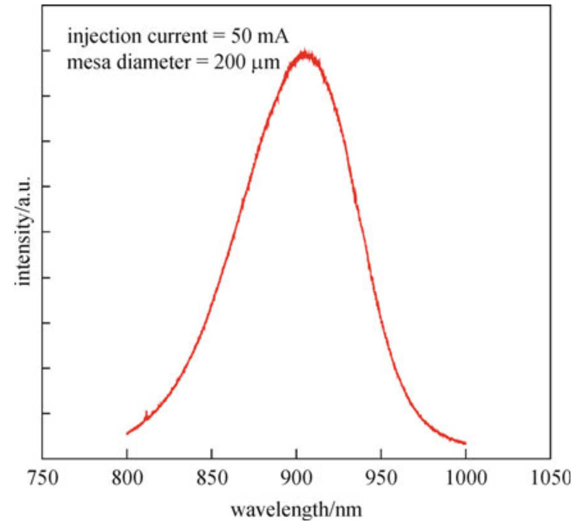

Fig. 10 Room temperature EL spectra of $In_{0.01}Ga_{0.99}As$/Ge/offcut Si LED

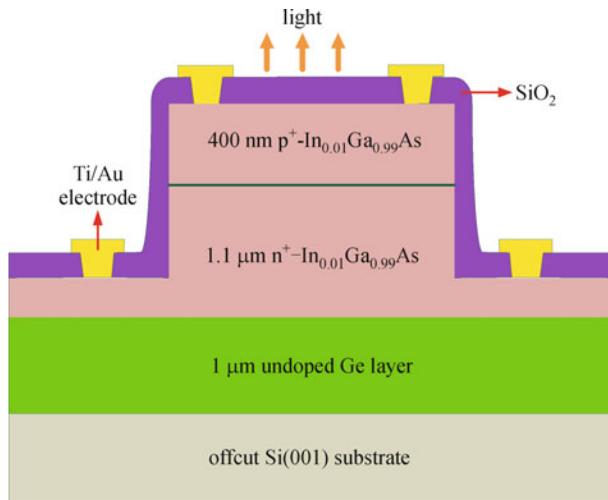

Fig. 9 Schematic cross-section view of $In_{0.01}Ga_{0.99}As$ LED

6 Epitaxy of GeSn on Ge/Si and GeSn photodetector

Group IV semiconductor $Ge_{1-x}Sn_x$ alloy has attracted considerable interest in the recent years for its potential applications in infrared photodetector and theoretically the direct band GeSn laser on Si. Theoretically, $Ge_{1-x}Sn_x$ alloy will become direct bandgap if Sn concentration x>10%, which makes it an exciting material potentially applied in Si-based laser [35]. Indirect bandgap semiconductor $Ge_{1-x}Sn_x$ alloys with $x < 10\%$ also have many applications. Even in the case of a very small Sn concentration (x~0.02), $Ge_{1-x}Sn_x$ alloy can cover all optical communication windows with a high absorption coefficient. Besides, in-plane tensile-strained Ge can be achieved on $Ge_{1-x}Sn_x$ alloys to improve the light emitting efficiency and carrier mobility of Ge. However, epitaxial growth of $Ge_{1-x}Sn_x$ alloys on Si is difficult. Firstly, Sn tends to segregate to the surface. Secondly, the equilibrium solid solubility of Sn in Ge is rather low ($x < 0.01$). Thirdly, there is a large lattice mismatch between GeSn and Si.

In order to overcome these difficulties, growth of $Ge_{1-x}Sn_x$ has to be proceeded under non equilibrium condition. Researchers at Arizona State University successfully grown high quality $Ge_{1-x}Sn_x$ alloys directly on Si(100) and Si(111), using SnD_4 and Ge_2H_6 as gas sources in a ultrahigh vacuum chemical vapor deposition (UHVCVD) system [36]. The growth temperature was 250°C–350°C. The Sn concentration decreased from 20% to 1% as the growth temperature elevated from 250°C to 350°C. Smooth $Ge_{1-x}Sn_x$ surface was obtained with R_{rms} of 0.5–1.4 nm. Secondary ion mass spectra (SIMS) and Rutherford back scattering (RBS) measurements indicated that Sn segregation was avoided. The $Ge_{1-x}Sn_x$ alloys was 93%–95% strain relaxed, with 0.25° FWHM of $Ge_{1-x}Sn_x$ X-ray diffraction (XRD) peak, and with a 10^5–10^6 cm^{-2} dislocation density.

Recently, we have obtained $Ge_{1-x}Sn_x$ alloys (x = 2.5%, 5.2% and 7.8%) on Si(001) substrates by MBE using high-quality Ge thin films as buffer layers [37]. The base pressure of the system was about 3.0×10^{-8} Pa. $Ge_{1-x}Sn_x$ alloys were grown by evaporating Ge and Sn (both 99.9999% pure) from PBN effusion cells. The 240 nm Ge buffer layer was grown by two-step process, in which a 40 nm thick Ge layer was deposited at 200°C, and subsequently a 200 nm thick Ge layer was grown at 500°C to obtain a high-quality Ge thin film. The R_{rms} was 1.27–2.15 nm and the FWHM of the $Ge_{1-x}Sn_x$ XRD peak is about 0.12°. The $Ge_{1-x}Sn_x$ alloys with x = 2.5%, 5.2% and 7.8%, were respectively estimated to be 100%, 98%

and 97.9% strained. RBS measurements confirmed the avoiding of Sn segregation. Thermal stability of $Ge_{1-x}Sn_x$ alloys were investigated by XRD and AFM, which indicated that $Ge_{1-x}Sn_x$ is stable at 500°C when the Sn concentration $x < 2.5\%$. Typical TEM images of $Ge_{1-x}Sn_x$ ($x = 7.8\%$) are shown in Fig. 11.

$Ge_{1-x}Sn_x$ alloys are recently applied in infrared photodetector [38,39]. By using a high quality 820 nm thick $Ge_{0.97}Sn_{0.03}$ alloy film grown on Si(001) by molecular beam epitaxy, we have successfully fabricated GeSn p-i-n photodetectors [23]. The schematic cross-section view of the detector is shown in Fig. 12. Circular mesas with diameters ranging from 20 to 200 μm were formed by etching the patterned films down to the Si substrate using an inductively coupled plasma etcher. For a 50 μm diameter device, the diode currents were 35.3, 45.2, and 534 μA at −1, 0, and 1 V, respectively. The measured dark current density was 1.8 A/cm^2 at −1 V. A disadvantage of Ge detector is the drastic decrease of the photoresponse of Ge detector beyond 1550 nm, which makes the device difficult to be applied in infrared region beyond 1550 nm. Comparing with the Ge detector, the responsivity of the GeSn detector decreases much slower and is higher beyond 1550 nm. Even at a wavelength as long as 1640 nm, the responsivity is still relatively high. At 1310, 1540, and 1640 nm, the responsivities are 0.52, 0.23, and 0.12 A/W, respectively, corresponding to external quantum efficiencies of 49.2%, 18.5%, and 9.1%. The responsivities spectra of the $Ge_{0.97}Sn_{0.03}$ detector under −1 V bias are shown in Fig. 13. The photocurrent spectrum measured at 0 V using a Fourier transform infrared spectrometer is also shown. As can be seen, the detectors exhibite relatively high responsivities in all the measured wavelengths (1310–1640 nm) and are shown to have a photoresponse up to 1800 nm, covering the whole telecommunication windows. The high performance of the $Ge_{0.97}Sn_{0.03}$ detector is guaranteed by the high quality Ge buffer layer, which enables the promising application for all telecommunication wavebands detection.

7 Conclusions

The significant progress of Ge-on-Si photonic devices makes it possible to realize Si-based monolithic optoelectronic integration. Nowadays, high performance Ge detector has been in practical used. Although the performances of Ge and Ge quantum well modulators till now are unable to meet the need of commercial application, the results have indicated the potential used in high speed optical communication and optical connection in the future. Despite the demonstrations of Ge LED and optical pump Ge laser recently, a great deal of research still has to be carried on to realize the continuous electric-pump Ge laser. By using Ge as buffer layer, high quality GaAs(InGaAs) and $Ge_{1-x}Sn_x$ can be epitaxy on Si. As a result, the advanced III-V photonic devices technology can be combined with the mature Si semiconductor process, and novel $Ge_{1-x}Sn_x$-on-Si infrared optical devices are expected.

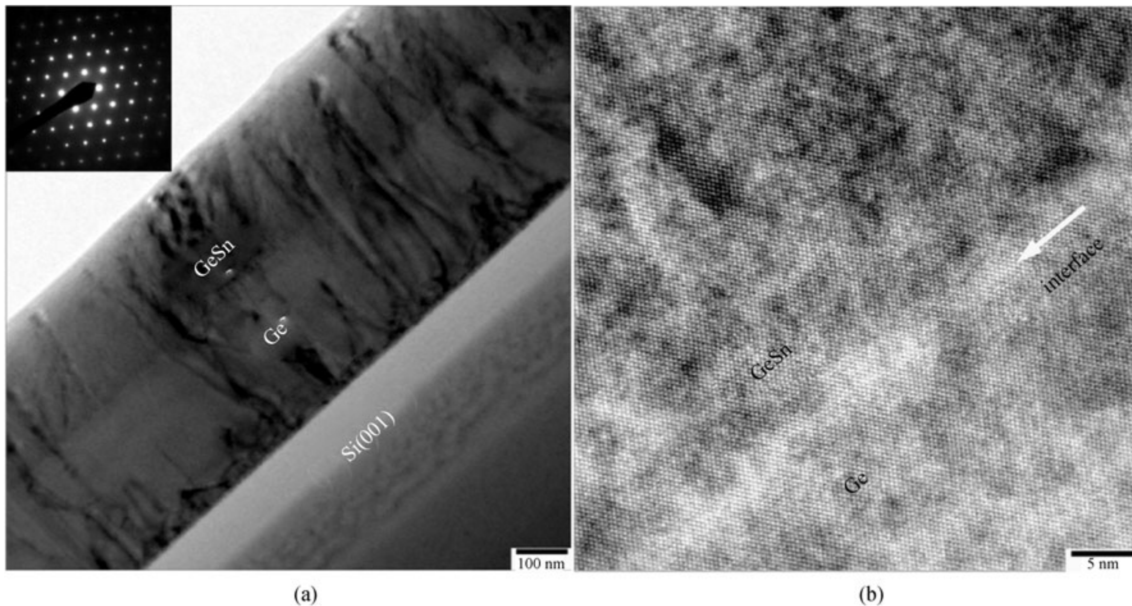

Fig. 11 (a) X-ray transmission electron microscope (XTEM) image of the $Ge_{0.922}Sn_{0.078}$ alloy; the inset is the selected area electron diffraction pattern taken from the $Ge_{0.922}Sn_{0.078}$ layer; (b) high resolution TEM micrograph of the $Ge_{0.922}Sn_{0.078}$/Ge interface

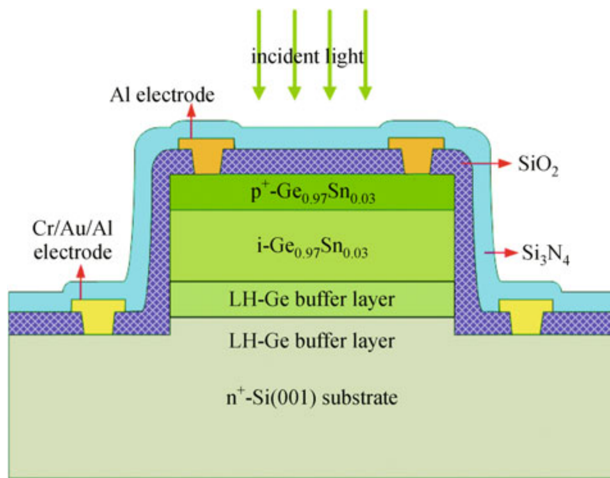

Fig. 12 Schematic cross-section view of $Ge_{0.97}Sn_{0.03}$ detector on Si

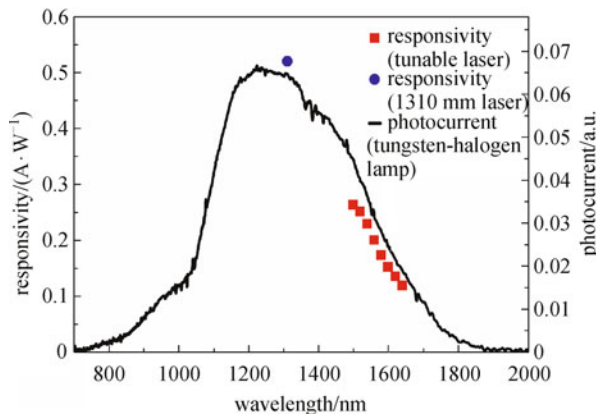

Fig. 13 Responsivity versus wavelength at –1 V along with photocurrent spectrum of a 100 μm diameter GeSn detector. The responsivities were measured using lasers while the photocurrent spectrum was measured at 0 V using a Fourier transform infrared spectrometer

Acknowledgements This work was supported by the National High Technology Research and Development Program of China (No. 2011AA010302), the National Natural Science Foundation of China (Grant Nos. 61036003, 61176013, 60906035, 61177038), and by Tsinghua National Laboratory for Information Science and Technology (TNList) Cross-discipline Foundation.

References

1. Jones R, Park H, Fang A W, Bowers J E, Cohen O, Raday O, Paniccia M J. Hybrid silicon integration. Journal of Materials Science Materials in Electronics, 2009, 20(S1): 3–9
2. Boyraz O, Jalali B. Demonstration of a silicon Raman laser. Optics Express, 2004, 12(21): 5269–5273
3. Rong H, Jones R, Liu A, Cohen O, Hak D, Fang A, Paniccia M. A continuous-wave Raman silicon laser. Nature, 2005, 433(7027): 725–728
4. Soref R, Bennett B. Electrooptical effects in silicon. IEEE Journal of Quantum Electronics, 1987, 23(1): 123–129
5. Halbwax M, Bouchier D, Yam V, Débarre D, Nguyen L H, Zheng Y, Rosner P, Benamara M, Strunk H P, Clerc C. Kinetics of Ge growth at low temperature on Si(001) by ultrahigh vacuum chemical vapor deposition. Journal of Applied Physics, 2005, 97(6): 064907
6. Liu J, Sun X, Pan D, Wang X, Kimerling L C, Koch T L, Michel J. Tensile-strained, n-type Ge as a gain medium for monolithic laser integration on Si. Optics Express, 2007, 15(18): 11272–11277
7. Chris G. Van de Walle. Band lineups and deformation potentials in the model-solid theory. Physical Review B: Condensed Matter and Materials Physics, 1989, 39(3): 1871–1883
8. Cheng T H, Peng K L, Ko C Y, Chen C Y, Lan H, Wu Y R, Liu C W, Tseng H H. Strain-enhanced photoluminescence from Ge direct transition. Applied Physics Letters, 2010, 96(21): 211108
9. Sun X, Liu J, Kimerling L C, Michel J. Direct gap photoluminescence of n-type tensile-strained Ge-on-Si. Applied Physics Letters, 2009, 95(1): 011911
10. Hu W, Cheng B, Xue C, Xue H, Su S, Bai A, Luo L, Yu Y, Wang Q. Electroluminescence from Ge on Si substrate at room temperature. Applied Physics Letters, 2009, 95(9): 092102
11. Sun X, Liu J, Kimerling L C, Michel J. Room-temperature direct bandgap electroluminesence from Ge-on-Si light-emitting diodes. Optics Letters, 2009, 34(8): 1198–1200
12. Cheng S L, Lu J, Shambat G, Yu H Y, Saraswat K, Vuckovic J, Nishi Y. Room temperature 1.6 μm electroluminescence from Ge light emitting diode on Si substrate. Optics Express, 2009, 17(12): 10019–10024
13. Liu J, Sun X, Camacho-Aguilera R, Kimerling L C, Michel J. Ge-on-Si laser operating at room temperature. Optics Letters, 2010, 35 (5): 679–681
14. Liu J, Beals M, Pomerene A, Bernardis S, Sun R, Cheng J, Kimerling L C, Michel J. Waveguide-integrated, ultralow-energy GeSi electro-absorption modulators. Nature Photonics, 2008, 2(7): 433–437
15. Feng N N, Feng D, Liao S, Wang X, Dong P, Liang H, Kung C C, Qian W, Fong J, Shafiiha R, Luo Y, Cunningham J, Krishnamoorthy A V, Asghari M. 30 GHz Ge electro-absorption modulator integrated with 3 μm silicon-on-insulator waveguide. Optics Express, 2011, 19(8): 7062–7067
16. Kuo Y H, Lee Y K, Ge Y, Ren S, Roth J E, Kamins T I, Miller D A B, Harris J S. Strong quantum-confined Stark effect in germanium quantum-well structures on silicon. Nature, 2005, 437(7063): 1334–1336
17. Zhao H W, Hu W X, Xue C L, Cheng B W, Wang Q M. Design of waveguide integrated Ge-quantum-well electro-absorption modulators. Chinese Physics Letters, 2011, 28(1): 014204
18. Chaisakul P, Marris-Morini D, Isella G, Chrastina D, Le Roux X, Gatti E, Edmond S, Osmond J, Cassan E, Vivien L. Quantum-confined Stark effect measurements in Ge/SiGe quantum-well structures. Optics Letters, 2010, 35(17): 2913–2915
19. Rong Y W, Ge Y S, Huo Y J, Fiorentino M, Michael R T T, Theodore I K, Tomasz J O, Guillaume H, James S H Jr. Quantum-confined Stark effect in Ge/SiGe quantum wells on Si. IEEE Journal

of Selected Topics Quantum Electronics, 2010, 16(1): 85–92

20. Mei X, Kabehie S, Stieg A Z, Tkatchouk E, Benitez D, Goddard W A, Zink J I, Wang K L. A molecular-rotor device for nonvolatile high-density memory applications. IEEE Electron Device Letters, 2010, 31(9): 1047–1049
21. Famà S, Colace L, Masini G, Assanto G, Luan H C. High performance germanium-on-silicon detectors for optical communications. Applied Physics Letters, 2002, 81(4): 586–588
22. Liu J F, Michel J, Giziewicz W, Pan D, Wada K, Cannon D D, Jongthammanurak S, Danielson D T, Kimerling L C, Chen J, Ömer Ilday F, Kartner F X, Yasaitis J. High-performance, tensile-strained Ge p-i-n photodetectors on a Si platform. Applied Physics Letters, 2005, 87(10): 103501–103502
23. Colace L, Balbi M, Masini G, Assanto G, Luan H C, Kimerling L C. Ge on Si p-i-n photodiodes operating at 10 Gbit/s. Applied Physics Letters, 2006, 88(10): 101111
24. Oehme M, Werner J, Kasper E, Klinger S, Berroth M. Photocurrent analysis of a fast Ge p-i-n detector on Si. Applied Physics Letters, 2007, 91(5): 051108
25. Park S B, Takita S Y, Ishikawa Y, Osaka J, Wada K. Reverse current reduction of Ge photodiodes on Si without post-growth anneling. Chinese Optics Letters, 2009, 7(4): 286–290
26. Xue H Y, Xue C L, Cheng B W, Yu Y D, Wang Q M. Zero biased Ge-on-Si photodetector with a bandwidth of 4.72 GHz at 1550 nm. Chinese Physics B, 2009, 18(6): 2542
27. Yin T, Cohen R, Morse M M, Sarid G, Chetrit Y, Rubin D, Paniccia M J. 31 GHz Ge n-i-p waveguide photodetectors on silicon-on-insulator substrate. Optics Express, 2007, 15(21): 13965–13971
28. Feng D Z, Liao S R, Dong P, Feng N N, Liang H, Zheng D W, Kung C C, Fong J, Shafiiha R, Cunningham J, Krishnamoorthy A V, Asghari M. High-speed Ge photodetector monolithically integrated with large cross-section silicon-on-insulator waveguide. Applied Physics Letters, 2009, 95(26): 261105–261107
29. Vivien L, Rouvière M, Fédéli J M, Marris-Morini D, Damlencourt J F, Mangeney J, Crozat P, El Melhaoui L, Cassan E, Le Roux X, Pascal D, Laval S. High speed and high responsivity germanium photodetector integrated in a silicon-on-insulator microwaveguide. Optics Express, 2007, 15(15): 9843–9848
30. Ahn D, Hong C Y, Liu J F, Giziewicz W, Beals M, Kimerling L C, Michel J, Chen J, Kärtner F X. High performance, waveguide integrated Ge photodetectors. Optics Express, 2007, 15(7): 3916–3921
31. Kang Y M, Liu H D, Morse M, Paniccia M J, Zadka M, Litski S, Sarid G, Pauchard A, Kuo Y H, Chen H W, Zaoui W S, Bowers J E, Beling A, McIntosh D C, Zheng X G, Campbell J C. Monolithic germanium/silicon avalanche photodiodes with 340 GHz gain–bandwidth product. Nature Photonics, 2009, 3(1): 59–63
32. Xue C, Xue H, Cheng B, Bai A, Hu W, Yu Y, Wang Q. In: 6th IEEE International Conference on Group IV Photonics. 2009, 178
33. Bolkhovityanov Y B, Pchelyakov O P. GaAs epitaxy on Si substrates: modern status of research and engineering. Physics-Uspekhi, 2008, 51(5): 437–456
34. Beeler R, Mathews J, e Weng C, Tolle J, Roucka R, Chizmeshya A V G, Juday R, Bagchi S, Menéndez JKouvetakis J. Comparative study of InGaAs integration on bulk Ge and virtual Ge/Si(1 0 0) substrates for low-cost photovoltaic applications. Solar Energy Materials and Solar Cells. 2010, 94(12):2362–2370
35. D’Costa V R, Cook C S, Birdwell A G, Littler C L, Canonico M, Zollner S, Kouvetakis J, Menéndez J. Optical critical points of thin-film $Ge_{1-y}Sn_y$ alloys: a comparative $Ge_{1-y}Sn_y/Ge_{1-x}Si_x$ study. Physics Review B, 2006, 73(12): 125207–125222
36. Bauer M, Taraci J, Tolle J, Chizmeshya A V G, Zollner S, Smith D J, Menendez J, Hu. C W, Kouvetakis J. Ge-Sn semiconductors for band-gap and lattice engineering. Applied Physics Letters, 2002, 81 (16): 2992–2994
37. Su S, Wang W, Cheng B, Zhang G, Hu W, Xue C, Zuo Y, Wang Q. Epitaxial growth and thermal stability of $Ge_{1-x}Sn_x$ alloys on Ge-buffered Si(001) substrates. Journal of Crystal Growth, 2011, 317 (1): 43–46
38. Su S, Cheng B, Xue C, Wang W, Cao Q, Xue H, Hu W, Zhang G, Zuo Y, Wang Q. GeSn p-i-n photodetector for all telecommunication bands detection. Optics Express, 2011, 19(7): 6400–6405
39. Mathews J, Roucka R, Xie J, Yu S Q, Menendez J, Kouvetakis J. Extended performance GeSn/Si(100) p-i-n photodetectors for full spectral range telecommunication applications. Applied Physics Letters, 2009, 95(13): 133506–133508